Self-Assembly of Three-Dimensional Nanostructured Antimony

Peng Liu,[†,*] Kuan Zhong,[†] Chaolun Liang,[‡] Qiqin Yang,[†] Yexiang Tong,[†,*] Gaoren Li,[†] and Greg A. Hope[§]

School of Chemistry and Chemical Engineering, Instrumental Analysis & Research Center, Sun Yat-Sen University, Guangzhou 510275, China, and School of Science, Griffith University, Nathan, Queensland 4111, Australia

Received January 26, 2008. Revised Manuscript Received October 30, 2008

The 3D nanostructured antimony is synthesized by simply immerging an anodically oxidized copper sheet into $SbCl_3$-$(n\text{-}Bu)_4NBF_4$-DMSO solution at room temperature. The morphology, shape, and structure were characterized by FE-SEM, XRD, and HRTEM. The 3D nanostructured antimony has a regular fourteen-faced polyhedron shape and is constructed by Sb nanowires. The Sb nanowires are single crystals with a rhombohedral crystal structure, the average diameter of the Sb nanowires ranges from 5 to 8 nm. The HRTEM investigation and theoretical calculations indicate that Sb nanowires grow along the arrises of its rhombohedral lattice. The growth mechanism is proposed, the electron transport along Sb nanowires may be anisotropic and results in the preferred orientation of the Sb nanowires growth. The nanocages can be formed by quaric self-assembly of Sb nanowires because of the anisotropy of its rhombohedral crystal structure.

1. Introduction

In the past two decades, nanostructured materials have received steadily growing attention not only because of their numerous properties and applications superior to those of their bulk counterparts but also because they can be used as good systems for theoretical study, such as examining electronic conduction and transport properties[1,2] and quantum confinement effects.[3,4] According to the architecture of these nanomaterials, they can be simply classified by their dimensionalities: zero-dimensional (0D) nanostructures (quantum dots) including nanoparticles of spheres, cubes; one-dimensional (1D) nanorods, nanowires, and nanobelts; two-dimensional (2D) nanostructures (quantum well), nanodiscs, and plates and other advanced shapes such as rod-based multipods and nanostars; three-dimensional (3D) nanonetworks. Nanomaterials with certain geometries exhibit unique shape-dependent characteristics and subsequent utilization as building blocks for the key components of nanodevices.[5] For example, 0D nanostructures have been extensively studied and a number of chemical methods have been developed for fabricating quantum dots with a variety of materials. With quantum dots as a model system, the evolution of their properties with size has been studied.[6] Many electronic, photonic, and magnetic devices can be organized by using quantum dots,[7] such as solar cells,[8] single-electron transistors,[9] and lasers.[10] 1D nanomaterials are of great interest in materials chemistry because they exhibit novel optical properties arising from dimensional anisotropy, and most importantly, they can be utilized as key materials in addressable two-terminal circuits for nanodevice applications. 2D nanostructures have also attracted current interest because they can be conveniently prepared using molecular beam epitaxy.[11] Among these nanomaterials, however, 3D nanostructures have rarely been reported. Recently, Yi and co-workers reported the synthesis of 3D networks constructed by PbSe nanowires.[12] The typical 3D nanostructures include carbon nanocages, metallofullerene and fullerene nanonetworks, polypyrrole nanonetworks, 3D superstructures and hollow nanoparticles.[13−18] To the best of our knowledge, 3D nano material with a regular shape of polyhedron with

* Corresponding author. E-mail: ceslp@mail.sysu.edu.cn.
† School of Chemistry and Chemical Engineering, Sun Yat-Sen University.
‡ Instrumental Analysis & Research Center, Sun Yat-Sen University.
§ Griffith University.

(1) Natelson, D. *Nat. Mater.* **2006**, *5*, 853.
(2) Zhang, Y.; Li, L.; Li, G. H.; Zhang, L. D. *Phys. Rev. B* **2006**, *73*, 113403.
(3) Sun, X. H.; Didychuk, C.; Sham1, T. K.; Wong, N. B. *Nanotechnology* **2006**, *17*, 2925.
(4) Heremans, J.; Thrush, C. M.; Lin, Y. M.; Cronin, S.; Zhang, Z.; Dresselhaus, M. S.; Mansfield, J. F. *Phys. Rev. B* **2000**, *61*, 2921.
(5) Jun, Y. W.; Seo, J. W.; Oh, S. J.; Cheon, J. *Coord. Chem. Rev.* **2005**, *249*, 1766.
(6) Nirmal, M.; Brus, L. M. *Acc. Chem. Res.* **1999**, *32*, 407.
(7) Barth, J. V.; Costantini, G.; Kern, K. *Nature* **2005**, *437*, 671.
(8) Huynh, W. U.; Dittmer, J. J.; Alivisatos, A. P. *Science* **2002**, *295*, 2425.
(9) Warburton, R. J.; Schäflein, C.; Haft, D.; Bickel, F.; Lorke, A.; Karrai, K.; Garcia, J. M.; Schoenfeld, W.; Petroff, P. M. *Physica E* **2001**, *9*, 124.
(10) Kazes, M.; Lewis, D. Y.; Ebenstein, Y.; Mokari, T.; Banin, U. *Adv. Mater.* **2002**, *14*, 317.
(11) Xia, Y.; Yang, P.; Sun, Y.; Wu, Y.; Mayers, B.; Gates, B.; Yin, Y.; Kim, F.; Yan, H. *Adv. Mater.* **2003**, *15*, 353.
(12) Jia, Z.; Hailin, P.; Candace, K. C.; Konrad, J.; Xiao, F. Z.; Yi, C. *Nano Lett.* **2007**, *7*, 1095.
(13) Saito, Y.; Matsumoto, T. *Nature* **1998**, *392*, 237.
(14) Tang, J.; Xing, G.; Zhao, Y.; Jing, L.; Gao, X.; Cheng, Y.; Yuan, H.; Zhao, F.; Chen, Z.; Meng, H.; Zhang, H.; Qian, H.; Su, R.; Ibrahim, K. *Adv. Mater.* **2006**, *18*, 1458.
(15) Haino, T.; Matsumoto, Y.; Fukazawa, Y. *J. Am. Chem. Soc.* **2005**, *127*, 8936.
(16) Acik, M.; Baristiran, C.; Sonmez, G. *J. Mater. Sci.* **2006**, *41*, 4678.
(17) Zhang, M.; Wang, Z.; Ma, D.; Zhang, R.; Qian, Y. *Aust. J. Chem.* **2005**, *58*, 539.
(18) Rapoport, L.; Bilik, Yu.; Feldman, Y.; Homyonfer, M.; Cohen, S. R.; Tenne, R. *Nature* **1997**, *387*, 791.

10.1021/cm802225h CCC: $40.75
Published on Web 12/03/2008

fourteen faces has not been reported. However, it is well-known that the size and shape of nano materials are key factors for the determination of their chemical and physical properties. Furthermore, Flemings proposed a tetrahedron with structure, properties, performance, and process at the four vertices to emphasized their mutuality.[19]

As a group VA element, antimony is a semimetal with an energy overlap of 180 mV between the conduction and valence bands at 4.2 K.[20] It is a valuable element in both fundamental research and practical applications because of its unique physical properties, including low carrier densities, long Fermi wavelength, and high carrier mobilities. For instance, the III−V Sb-based semiconductor plays an important role in electronics, optoelectronics and thermoelectric materials.[21] In particular, the finite-size effect and quantum confinement effect are expected to be observed in Sb nanowires and the transport properties of these nanowires strongly depend on the diameter and the crystal orientation of nanowires.[22,23] Antimony and bismuth nanowires have drawn special attention because their small effective mass and large mean-free path make these nanowires make an interesting system for studying quantum confinement effects.[24] In addition, these nanostructured semimetals could exhibit even more interesting electronic properties,[25,26] such as surface superconductivity, extremely large magnetoresistance, semimetal to semiconductor transition, and high-efficiency thermoelectricity generation. In recent years, Sb nanowires have been fabricated by pulsed electrodeposition[27] and the vapor phase deposition[23] in anodic alumina membranes, self-assembly on graphite,[28]solvothermal synthesis,[29,30] and electrodeposition.[31,32] The transport properties of Sb nanowires have also been studied.[2]

In this paper, we report the synthesis and characterization of the 3D Sb nanocages, which are constructed from Sb nanowires with a fourteen-faced polyhedron structure. Cages form following immersion anodically oxidized Cu sheet into $SbCl_3$−DMSO solution at room temperature. A probable growth mechanism is discussed.

(19) National Research Council. *Materials Science and Engineering for the 1990s−Report of the Committee on Materials Science and Engineering*; National Academy Press: Washington, D. C., 1989. 29−270.
(20) Windmiller, L. R. *Phys. Rev.* **1966**, *149*, 472.
(21) Prieto, A. L.; Martín-González, M.; Keyani, J.; Gronsky, R.; Sands, T.; Stacy, A. M. *J. Am. Chem. Soc.* **2003**, *15*, 2388.
(22) Heremans, J.; Thrush, C. M.; Lin, Y. M.; Cronin, S. B.; Dresselhaus, M. S. *Phys. Rev. B* **2001**, *63*, 085406.
(23) Barati, M.; Chow, J. C. L.; Ummat, P. K.; Datars, W. R. *J. Phys.: Condens. Matter* **2001**, *13*, 2955.
(24) Huber, T. E.; Graf, M. J.; Foss, C. A., Jr.; Constant, P. *J. Mater. Res.* **2000**, *15*, 1816.
(25) Heremans, J. P.; Thrush, C. M.; Morelli, D. T.; Wu, M. C. *Phys. Rev. Lett.* **2002**, *88*, 216801.
(26) Yang, F. Y.; Liu, K.; Hong, K.; Reich, D. H.; Searson, P. C.; Chien, C. L. *Science* **1999**, *284*, 1335.
(27) Zhang, Y.; Li, G.; Wu, Y.; Zhang, B.; Song, W.; Zhang, L. *Adv. Mater.* **2002**, *14*, 1227.
(28) Wang, X. S.; Kushvaha, S. S.; Yan, Z.; Xiao, W. *Appl. Phys. Lett.* **2006**, *88*, 233105.
(29) Wang, Y. W.; Hong, B. H.; Lee, J. Y.; Kim, J. S.; Kim, G. H.; Kim, K. S. *J. Phys. Chem. B* **2004**, *108*, 16723.
(30) Zhang, W. Q.; Xu, L. Q.; Xi, G. C.; Wu, W. C.; Qian, Y. T. *Chem. Lett.* **2004**, *33*, 1476.
(31) Wu, J. Hl; Yan, J. W.; Xie, Z. X.; Xue, Q. K.; Mao, B. W. *J. Phys. Chem. B* **2004**, *108*, 2773.
(32) Huang, X. H.; Zhu, Y. G.; Dou, X. C.; Li, G. H. *Mater. Lett.* **2008**, *62*, 249.

2. Experimental Section

All chemical reagents used are analytically pure. DMSO was purified by reduced pressure distillation. $SbCl_3$ was dehydrated at 328 K under vacuum for 8 h. Cu sheets (99.99%) were polished and then undergone anodic oxidation at the potential of 0.1 V (vs saturated calomel electrode) in 1×10^2 mol m^{-3} H_2SO_4 solution for 30 min.

Synthesis of Three-Dimensional Nanostructured Antimony. After being anodic oxidized the Cu sheet was simply immerged into $SbCl_3$−(n-Bu)$_4$NBF$_4$−DMSO solution at room temperature and the Sb nanocage grows on the Cu substrate by self-assembly. (n-Bu)$_4$NBF$_4$ was used as a supporting electrolyte to increase the electric conductance of the DMSO solution. The Cu substrate was removed from the DMSO solution and washed by DMSO and acetone, respectively.

Characterization Methods. The field-emission scanning electron microscope (FE-SEM) images were obtained on a JSM-6330F scanning electron microscope (JEOL Ltd.). The composition of the samples was analyzed by energy dispersive X-ray spectrometer (EDS) with a Link-ISIS-300 (Oxford). The atomic force microscope (AFM) images were obtained on a SPM-9500J3 (Shimadu Precision Instruments, Inc.). The high-resolution transmission electron microscopy (HRTEM) and selected area electron diffraction (SAED) patterns were performed with a JEM-2010HR (JEOL Ltd.) operated at an accelerating voltage of 200 kV. For TEM, the samples underwent ultrasonic treatment and were prepared by dispersion in ethanol with brief sonication followed by drop-casting on a lacey carbon-coated grid (Electron Microscopy Sciences, LC200-Cu, Mesh 200). The X-ray diffraction (XRD) experiment was carried out using a D-MAX 2200 VPC diffractometer (RIGAKU) with Cu Kα_1 radiation, acceleration voltage was 40 kV with a 30 mA current flux.

3. Results and Discussion

The deposit formed on the surface of the copper sheet was analyzed by energy dispersive X-ray spectroscopy (EDS), X-ray diffraction (XRD) and selected area electron diffraction (SAED), the results identified that the deposit was Sb. The electrode potentials were measured in the solution mentioned above, the result confirmed that the sequence of electrode potentials is $\varphi(Sb^{3+}/Sb) > \varphi(Cu^{2+}/Cu)$, and thus the following reaction should occur

$$2Sb^{3+} + 3Cu = 2Sb + 3Cu^{2+} \quad (1)$$

Figure 1 presents the XRD pattern obtained from an as-deposited sample. The diffraction peaks of Sb were observed, these diffraction peaks belong to the facets $(01\bar{1}2)$, $(10\bar{1}4)$, $(11\bar{2}0)$, and $(20\bar{2}2)$ of Sb rhombohedral crystal (indexed as a hexagonal system). Thus the deposit is antimony with a rhombohedral lattice. It should be noted that the intensity of the diffraction peak $(20\bar{2}2)$ is more intense than the weak peak $(20\bar{2}2)$ indicated in the pdf entry (JCPDS 35−0732).

Figure 2a is a typical field-emission scanning electron microscope (FE-SEM) image of the deposit, showing the morphology resembling a nestlike 3D nano structure. The average diameter of the Sb nanowires was calculated less than 10 nm and the average diameter of the nanaocages is about 1800 nm from a higher resolution SEM image. It is more interesting that these nests formed by the nanowires have a regular fourteen-faced polyhedron shape as shown

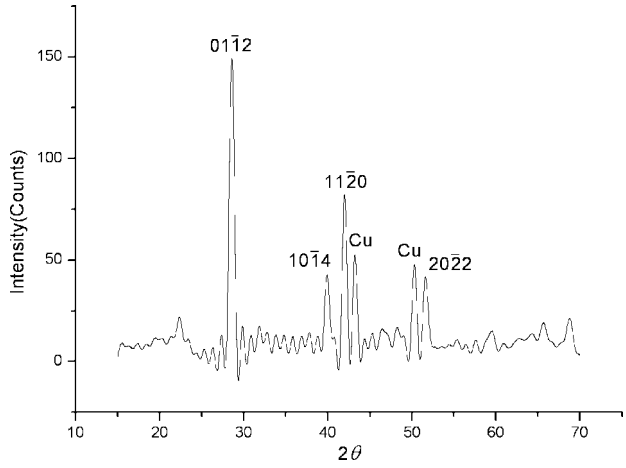

Figure 1. XRD pattern of the sample obtained in $SbCl_3$(10 mol m^{-3})−(n-Bu)$_4NBF_4$ (1×10^2 mol m^{-3})−DMSO for 30 min, 30 °C.

in the inset of Figure 2a. The AFM image of the sample is shown in figure 2b, it presents a good view in three dimensions and confirms the structure mentioned above. Nanowire and nanowire arrays fabricated by using the synthesis on templates and self-assembly or self-organization processes are very common, but nanowires assembled into 3D nanostructure are infrequent. Our experiment indicated that the antimony nanowires grew along a preferred orientation by self-assembly and nestlike nanocages with fourteen faced polyhedron can be formed by quadric self-assembly of Sb nanowires.

A transmission electron microscopy (TEM) image of the sample after ultrasonic treatment is shown in Figure 3a, a fragment of the nanocages was captured. The nanowires grew in length and breadth and intersect at a regular angle to generate many parallelogrammical patterns. The diameter of the nanowires ranges from 5 to 8 nm. Inspection of the Sb mesh structures confirmed that the nanocages were pleached by nanowires, this is further confirmed by the AFM image of the crashed nanocage (see the Supporting Information). The inset in Figure 3a is a selected area electron diffraction (SAED) pattern from the circle region in the TEM image. The reflections correspond to (10$\bar{1}$1), (10$\bar{1}$4), and (0003) planes of crystalline Sb having a rhombohedral crystal structure. The corresponding high-resolution transmission electron microscopy (HRTEM) is shown in Figure 3b; the area in which the lattice fringe image appeared reveals the orientation, size, and grain boundary of the nanowires, which corresponds to the parallelogrammical patterns in Figure 3a. Therefore, we can conclude that the Sb nanowires grow as a single crystal.

To investigate the growth direction of these Sb nanowires, we studied the HRTEM image of a single nanowire segment. Figure 3c shows the TEM image of the Sb nanowire segment, the orientation of the nanowire can be clearly seen. Figure 3d is the HRTEM image of the top region of the Sb nanowire, the lattice image appeared. Figure 3e is the diffractogram obtained by fast Fourier transform from the square region in Figure 3d. The diffraction pattern can be indexed as the diffraction along the [4$\bar{5}$1$\bar{3}$] zone axis of single-crystalline Sb with rhombohedral structure. The Fourier-filtered reconstructed image from the square region in Figure 3d is shown in Figure 3f. (10$\bar{1}$1) planes can be indexed, which is in accord with the diffractogram in Figure 3e. Therefore, the Sb nanowires were formed by the stacking of (10$\bar{1}$1) planes. The (10$\bar{1}$1) planes in a hexagonal system can be transformed into (100) planes in a rhombohedral system, and thus we conclude that Sb nanowires grew along the arrises of the rhombohedral lattice, as shown in Figure 3g. These HRTEM results correspond with XRD results mentioned above, in which the increasing intensity of the (20$\bar{2}$2) peak is due to the preferential growth of the Sb nanowires along the corresponding direction.

To further explore the mechanism of the Sb nanocages growth, experiments under different conditions and different growth stages were carried out and various morphologies of the Sb deposits were observed, as shown in Figure 4. Figure 4a shows the dendritic structure assembled by Sb nanowires, the broad nanowires can be defined as trunks and there are many nodes on the trunks, a pair of nanowires branches grew up at each node. Each pair of the branches and the trunk itself constitute a trigonal axis structure. The typical structure can be abstractly illustrated in figure 5a; These trigonal axis can also be observed in Figure 4b. Three Sb nanowires (the arrises of the triangular pyramid structure) grew from the apex. Two branches grew at different nodes (similar to the structure in figure 4a) on each arris. These nanowires form the 3D nano structure, i.e., the triangular pyramidial structure. The typical structure can be abstractly illustrated in Figure 5b; In Figure 4c, the triangular pyramidial structure can be observed, two triangular pyramids shared a common arris (edge sharing), as illustrated in Figure 5c; the basic structure units as shown in parts b and c in Figure 5 are very common and can be observed in many SEM images of different samples (Figure 2 in the Supporting Information). These basic structure units are different from the nanocages. They look like the substructures or the primary structures of nanocages, in other words, these units may present the progress of the nanocages growth. Figure 4d shows the complete nanocage with a fourteen faced polyhedron, as illustrated in Figure 5d. On each face of the fourteen-faced polyhedron, there are many parallelograms formed from regularly intersecting Sb nanowires, as shown in Figure 5e. These proposed parallelogram patterns are consistent with the TEM observations. By analyzing the different structures shown in Figure 5, it can be found that these structures involve a common and basic configuration unit: three nanowires that grow along the arrises of a triangular pyramid, as shown in Figure 5f. The structures shown in Figure 5a−d can be obtained by repeating this configurational unit.

Fractal structure is very common in the natural world. Many phenomena in the fields of science and technology exhibit noninteger (or fractal) dimensionality as was recognized by Mandelbrot in his work.[33] Nanostructured dendrites, as a kind of fractal structure, have been prepared using different methods. For the formation of fractal structure, there are many reports both on the theoretical and experimental aspects. It is believed[34] that the ions were reduced to atoms in solution and these atoms aggregated to clusters or particles via diffusion and bump, the aggregation clusters accumulate

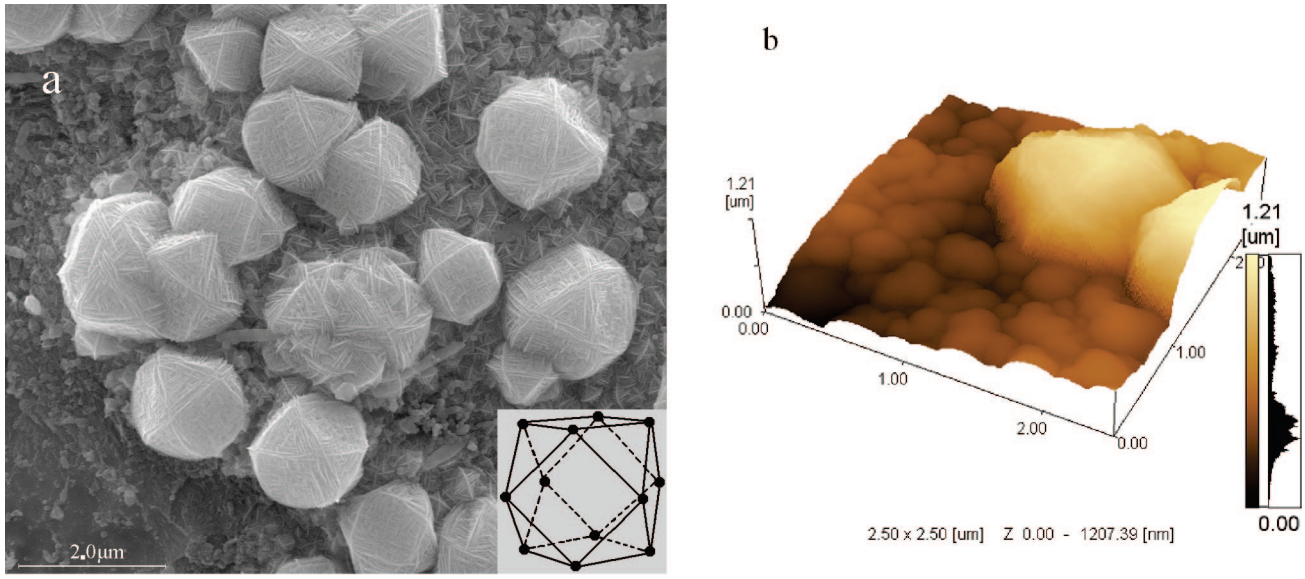

Figure 2. Typical FE-SEM and AFM images of the sample obtained in $SbCl_3$(10 mol m^{-3})−(n-Bu)$_4NBF_4$ (1 × 10^2 mol m^{-3})−DMSO for 30 min, 30 °C. The Cu sheet was pre-electrooxidized in 1 × 10^2 mol m^{-3} H_2SO_4 solution at the potential of 0.1 V for 30 min.

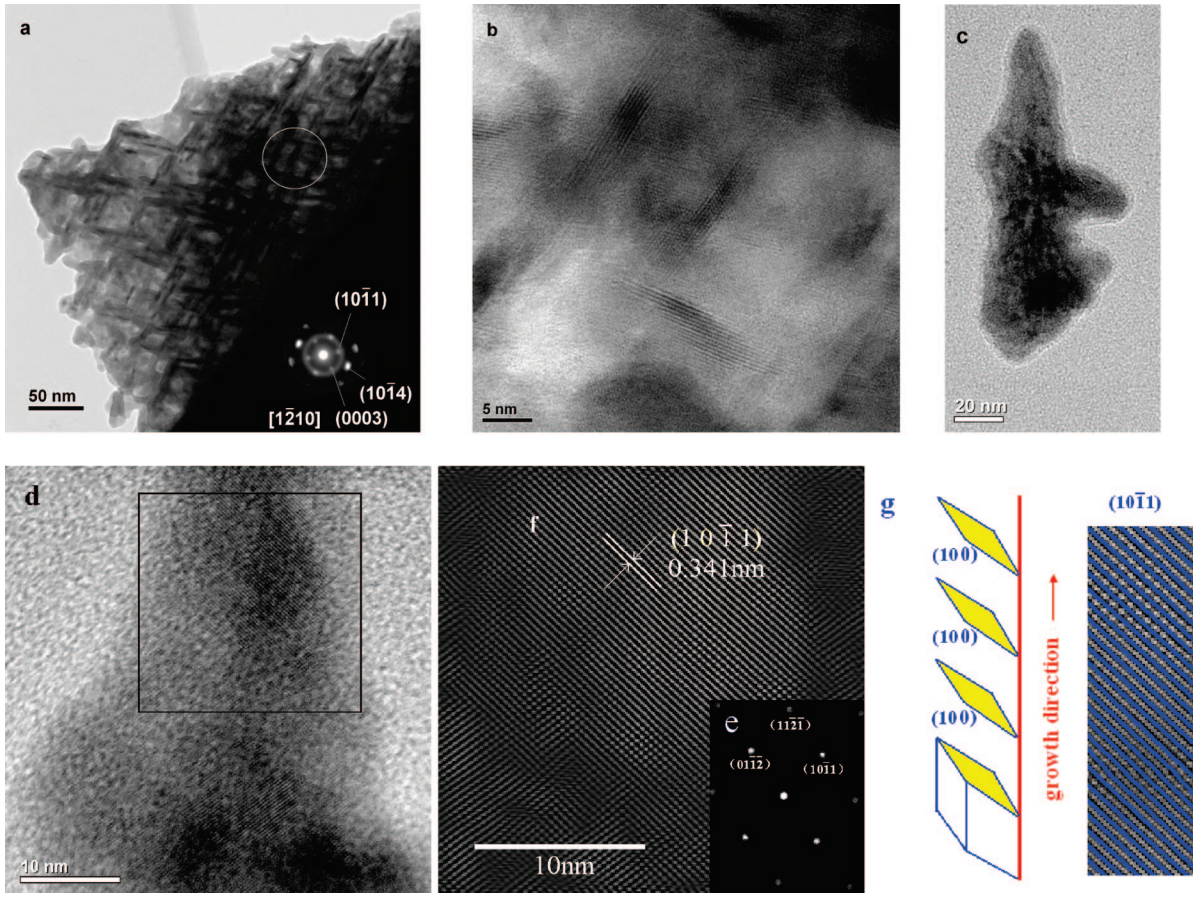

Figure 3. (a) TEM image and SAED pattern, (b) HRTEM image from the circle region in (a). (c) TEM image, (d) HRTEM image of the Sb nanowire segment. (e) Diffractogram obtained by fast Fourier transform, (f) Fourier-filtered reconstructured image from the square region in (d). (g) Sketch map of the nanowire growth direction. The sample was obtained in $SbCl_3$(10 mol m^{-3})−(n-Bu)$_4NBF_4$ (1 × 10^2 mol m^{-3})−DMSO for 30 min, 30 °C.

to a crystal seed on contact along the preferred direction, because of the intrinsically strong crystalline anisotropy. Anisotropy, which plays a key role in the formation of dendrite, may come from the interaction between the background and aggregating particles or the anisotropy of the growing crystalline nanoparticles.

(33) *The Fractal Geometry of Nature*; Mandelbrot, B. B., Ed.; Freeman: New York, 1982.

(34) Yang, B.; Wu, Y.; Hub, H.; Li, C.; Yang, X.; Qian, Y. *Mater. Chem. Phys.* **2005**, *92*, 286.

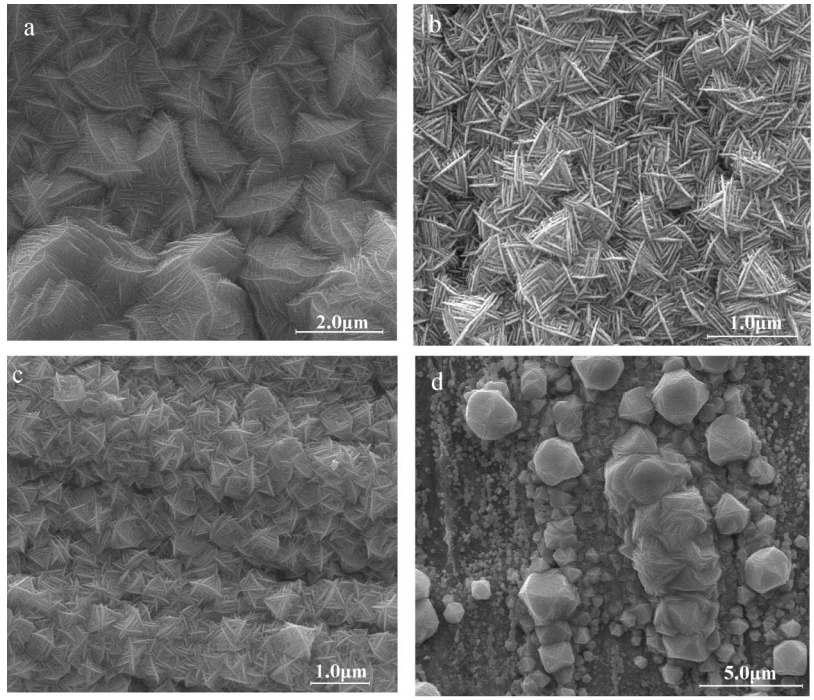

Figure 4. SEM images of Sb samples grown in $SbCl_3$(10 mol m^{-3})−(n-Bu)$_4NBF_4$ (1×10^2 mol m^{-3})−DMSO solution at different conditions, Cu substrate was anodically oxidized for 10 min and immersed in the solution at 30 °C for (a) 15, (b) 30, (c) 45, and (d) 30 min.

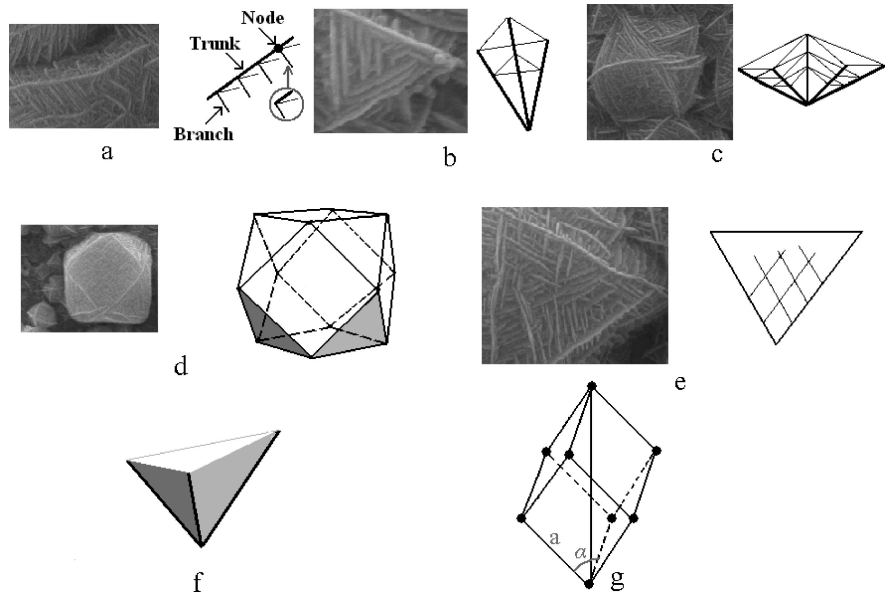

Figure 5. Typical morphologies and their illustrations of the samples derived from Figure 4.

Xia and co-workers[11] reviewed the generation of 1D nanostructures via variety of chemical and vapor phase methods. They broadly divided the formation of nanowires into three categories: (a) anisotropic growth is dictated by the linear, crystallographic structure of a solid material; (b) anisotropic growth is directed or confined by a template; and (c) anisotripic growth is kinetically achieved by controlling the supersaturation or through the use of an appropriate capping reagent. The essence of nanowire growth is about crystallization, the formation of a solid from a vapor, liquid, or solid phase can be roughly described as two fundamental steps: nucleation and growth. As the basic units (atoms, ions, or molecules), which can be used to constitute a crystal, were generated, they combine into nuclei through homogeneous nucleation. These nuclei can serve as seeds for further growth to form larger structures. However, if there is an anisotropic effect that affects the further growth of the seeds, the formation of 1D nanostructures can be expected.

In summary, according to the reports both on the growth mechanism and experimental methods of 1D nanostructures, there is no doubt that the generation or introduction of anisotropic effect during the growth of the crystal is the key for the preparation of 1D nanostructures.

For antimony, besides the underlying anisotropy of its crystal structure, other anisotropic properties had been reported. Many years ago, the studies of anisotropic self-diffusion, such as antimony[35] and bismuth,[36] had shown the anisotropy in the diffusion coefficient between the directions

of perpendicular and parallel to the trigonal axis of the rhombohedral lattice; Hatta and Mukasa[37] investigated the electron tunneling on Al/Al oxide/Sb tunnel junction with a different exposed dominant crystal face, the anisotropic effect of electron tunneling (the change in shape of the tunnel conductance) was observed; Zhang and co-workers[2] found the existence of the transition from a positive temperature coefficient of resistance to a negative one with decreasing diameter of the Sb nanowires. The electrical transport properties of Sb nanowires strongly depend on the crystal orientation and the diameter of nanowires.

In our experiment, we observed the following fact: Sb atoms did not pile along two dimensions and cover the whole surface of the copper substrate, instead they grew along a single preferred direction and Sb nanowires were formed by self-assembly, these nanowires constructed the Sb nanocages by quadric self-assembly. Obviously this phenomenon results from the characteristics of the displacement reaction and the crystal structure of antimony. The regular fourteen-faced polyhedron shape of Sb nanocage exhibits the self-modeling properties of the crystal growth. Antimony has a rhombohedron structure with the lattice parameters of $a = 4.301$ Å, $b = 4.301$ Å, and $c = 11.23$ Å (JCPDS 35−0732, indexed as a hexagonal crystal system), as shown in Figure 5g.

According to the analysis mentioned above, we hypothesized that the electrons (derived from the copper oxidation reaction) transport through the Sb deposit anisotropically: the electron is apt to transport along the three arrises of the Sb rhombohedral lattice. Sb^{3+} tends to obtain electron at the tips of the arrises and the reduced Sb metal accumulates along the arrises to form the nanowire. This hypothesis is supported by the HRTEM results: Sb nanowires grew along the trigonal axes of a rhombohedral lattice. Therefore, we proposed the following mechanism to explain the growth of Sb nancage.

The Cu substrate underwent anodization and the oxide film was generated on the surface. EDS and XPS experiment showed that the compositions of the oxide film are Cu_2O and CuO (see the Supporting Information). The FE-SEM observation indicated there were irregular and stochastic holes on the surface of Cu substrate (see the Supporting Information); the holes were caused by the anodic stripping of copper. A large portion of bare Cu surface was covered by copper oxide film, which was formed by passivation. We found that Sb nanocages could not grow on the Cu substrate which was not anodically oxidized. Generally, the process of anodic oxidization involves two aspects: anodic stripping and passivation. The holes were caused by anodic stripping and bare copper still existed at the end of the holes, whereas the oxide film, which covered a large portion of Cu surface, was caused by the passivation. In the system the reactive species were Cu(0) and Sb^{3+}, the productions were determined as Sb, so replacement reaction must occur. The oxide film could not react with Sb^{3+}. Therefore the replacement reaction occurred in the holes (the active centers) and the holes acted as a "hard template" to confine the growth of the nanostructured Sb. At the beginning of the reaction, Cu lost electrons and Sb^{3+} got electrons to form the crystal seeds. These seeds occupied the active centers. With the progress of the reaction, the Sb^{3+} nearby Cu(0) in the hole was exhausted. Although the holes were covered by the Sb crystal seed, there was still electrolyte (with low concentration of Sb^{3+}) in the holes and micro-Galvanic cells can operate with two electrode−electrolyte interfaces, i.e., $Cu-Cu^{2+}$ and $Sb-Sb^{3+}$. The deposited Sb acted as lead wire to transport electron. The reaction proceeded like the typical Galvanic cell. When Sb^{3+} ions adsorbed onto the Sb crystal seeds, Cu atoms at the roots of the Sb crystal seeds lost electrons according to the oxidation reaction: $Cu = Cu^{2+} + 2e^-$, then the electrons pass through Sb crystal seeds, with the adsorbed Sb^{3+} obtained the electrons at the surface of Sb crystal seeds and the reduction reaction $Sb^{3+} + 3e^- = Sb$ occurred. The copper sheet was the anode and was in electrical contact with the tips of Sb crystal seeds that formed the cathode. Because of the good electron transport along the arrises of the Sb rhombohedral crystal, these locations were preferred reduction regions and Sb atoms accumulated along this preferential orientation to form nanowires, as shown in Figure 6a.

The displacement reaction results in the Sb deposition and this process can be regarded as numerous tiny Daniel cells reacted on the surface of the anodized copper substrate, the cathodic areas are the growth sites of Sb nanowires. Therefore, the growth of Sb nanowires follows the electrochemical model, i.e., the electrodeposition without an external power supply, the so-called dip coating or immersion plating. This is different from the generating of nanowires via common chemical methods, so the growth of Sb nanowires follows the "electrochemical mode".

The accumulating speed of Sb atoms along the three arrises of the Sb crystal seeds is preferred, therefore the Sb nanowires are apt to grow along the arrises direction, these arrises can be called trunks. Whereas Sb nanowires can also grow along the arrises direction at different points on the trunks, these nanowires can be called branches and the points can be called nodes. In a word, the growth of Sb nanowires has a character that grew along the arrises of the Sb rhombohedral lattice. This mechanism can explain the growth of all the nanostructures observed in the SEM images. If the Sb crystal seed that was formed at the beginning of the replacement reaction lay in the small holes, as shown in Figure 6b, the growth along the two arrises, which were close to the substrate, was prohibited because of the confinement of the hole. Thus, the growth along the third arris (or the trunk) was dominate. During the nanowire growth along the trunk, at the node on the trunk a pair of nanowires (or the branches) grew along the other two arrises. As shown in Figure 6c, this was caused by the preferential growth along arrises. This dendritic structure can be found in Figure 5a. If the orientation of Sb crystal seeds is erect in the holes, as shown in Figure 6d, Sb nanowires could grow along three trunks, see Figure 6e. Similarly, branching nanowires grew along the arrises at different nodes on each trunks, as shown in Figure 6f, so the parallelograms on the triangular plane of the pyramidial were formed in this manner. However, the branching nanowires could also grow along the reverse

(35) Huntingtong, H. B.; Ghate, P. B.; Rosolowski, J. H. *J. Appl. Phys.* **1964**, *35*, 3027.
(36) Seith, W. *Z. Elektrochem. Angew. Phys. Chem.* **1933**, *39*, 538.
(37) Hatta, E.; Mukasa, K. *Solid State Commun.* **1996**, *98*, 293.

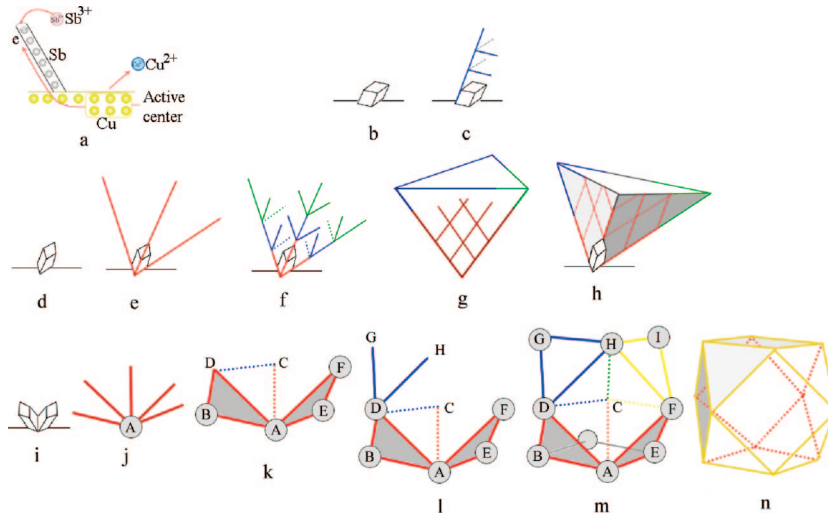

Figure 6. Sketch map of the Sb nanocage growth mechanism.

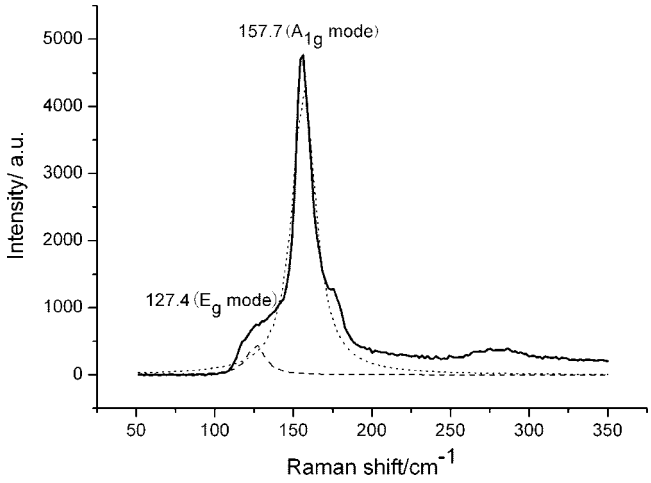

Figure 7. Room-temperature Raman spectrum of the Sb nanocages and the corresponding Lorentz fits (dash line).

direction of the arrises and, in this way, the closed triangular pyramidial structure was formed, as shown in g and h in Figure 6. This structure can be found in the SEM image in Figure 5e. If the two Sb crystal seeds had the same arris, as shown in Figure 6i, five nanowires could grow along the five trunks, as shown in Figure 6j. The branching nanowires could grow along the arrises at many different nodes on each trunks. As mentioned above, the branching nanowires could also grow along the reverse direction of the arrises. For example, at point D, the nanowires DB, DC, and DA grew up and DB, DC, and DA constituted the three arrises of the triangular pyramid, as shown in Figure 6k. Nanowires DG and DH grew along the other two arrises and the two triangular pyramids have the same arris DC, as shown in Figure 6l. Likewise, at point F, nanowires FH and FI grew along the arris direction, as shown in Figure 6m. The same manner was repeated and a nanocage with a fourteen-faced polyhedron was formed, as shown in Figure 6n.

To examine the nanosize effect of the Sb nanocage, the Raman spectrum of the as-prepared antimony nanocages was carried out and presented in Figure 7. It was reported that the two first-order Raman modes: E_g mode of the bulk trigonal Sb is at 117 cm^{-1}, A_{1g} mode at 152 cm^{-1},[38] and a broad weak peak between 250 and 300 cm^{-1} can be attributed to second-order scattering by optical phonon modes.[39]

However, the E_g and A_{1g} modes of the Sb nanocages are at 127.4 and 157.7 cm^{-1}, respectively. The blue shift of the Raman lines (especially E_g mode) of Sb nanocages was observed. It had been reported[40] that the phonon dispersion is the function of wavevector q and confinement leads to a transfer of q value. In the specific case of nanostructured antimony, the blue-shift in Raman lines is because of the decrease of the phonon dispersion of the Sb nanocage with the q value. The Raman spectrum reveals that the as-prepared antimony nanocages are nano structured. No more other peaks could be observed at the region over 1000 cm^{-1}. Among the Raman shift peaks of the samples, the dominated peak at 157.7 cm^{-1} has the stronger intensity and narrower line-width, no impurity relevant Raman peaks appeared in the Raman spectrum, which indicates that the samples are composed of pure antimony with good crystal quality of the rhombohedral structure.

In summary, the 3D nanostructured antimony can be simply synthesized by the displacement reaction $2Sb^{3+} + 3Cu = 2Sb + 3Cu^{2+}$. The growth mechanism is attributed to the anisotropic electron transport along Sb nanowires. This suggests that the 3D nano structure may be a good system for studying the electronic conduction and transport properties and quantum confinement effects.

Acknowledgment. This work was supported by the National Nature Science Foundation of China (Grant 20573136), China-Australia Special Fund for Scientific and Technological Cooperation (Grant 20711120186), and Guangdong Natural Science Foundation (Grant 8151027501000095).

Supporting Information Available: The AFM image of the crashed nanocage, the SEM images of the nanostructured antimony at different growth stage, XPS spectra, and SEM image of the anodized Cu sheet (PDF). This material is available free of charge via the Internet at http://pubs.acs.org.

CM802225H

(38) Sharp, R. I.; Warming, E. *J. Phys. F: Met. Phys.* **1971**, *1*, 570.

(39) Lannin, J. S.; Calleja, J. M.; Cardona, M. *Phys. Rev. B* **1975**, *12*, 585.

(40) Roy, A.; Komatsu, M.; Matsuishi, K.; Onari, S. *J. Phys. Chem. Solids* **1997**, *58*, 741.